Chaotic convection in an Oldroyd viscoelastic fluid in saturated porous medium with feedback control

Cite as: Chaos **30**, 073109 (2020); doi: 10.1063/5.0002846
Submitted: 28 January 2020 · Accepted: 15 June 2020 ·
Published Online: 6 July 2020

View Online Export Citation CrossMark

M. N. Mahmud,[1] Z. Siri,[2] J. A. Vélez,[3] L. M. Pérez,[3] and D. Laroze[3,a)]

AFFILIATIONS

[1]Malaysian Institute of Chemical & Bioengineering Technology, Universiti Kuala Lumpur, 78000 Alor Gajah, Malaysia
[2]Institute of Mathematical Sciences, University of Malaya, 50603 Kuala Lumpur, Malaysia
[3]Instituto de Alta Investigación, CEDENNA, Universidad de Tarapacá, Casilla 7D, Arica, Chile

Note: This article is part of the Focus Issue, instabilities and Nonequilibrium Structures.
a)**Author to whom correspondence should be addressed:** dlarozen@uta.cl

ABSTRACT

The control effects on the convection dynamics in a viscoelastic fluid-saturated porous medium heated from below and cooled from above are studied. A truncated Galerkin expansion was applied to balance equations to obtain a four-dimensional generalized Lorenz system. The dynamical behavior is mainly characterized by the Lyapunov exponents, bifurcation, and isospike diagrams. The results show that within a range of moderate and high Rayleigh numbers, proportional controller gain is found to enhance the stabilization and destabilization effects on the thermal convection. Furthermore, due to the effect of viscoelasticity, the system exhibits remarkable topological structures of regular regions embedded in chaotic domains.

Published under license by AIP Publishing. https://doi.org/10.1063/5.0002846

Thermal convection of viscoelastic fluids in a porous medium is studied as it exhibits complex dynamical behaviors. In particular, this kind of system can lead to chaotic states. One interesting question is how to control its chaos. Several methods, such as feedback control, have been applied. In this work, we consider the effect of the feedback control on the convection of a viscoelastic fluid. We derive a generalized Lorenz system that makes the system understandable in a simpler manner. Different numerical indicators are employed to characterize the system's states. Feedback control allows the switching between chaotic and regular states.

I. INTRODUCTION

Thermal convective instability in a fluid-saturated porous medium has drawn substantial interest over the last few years due to its various physical and technical applications such as geophysics, building thermal insulation, petroleum reservoir modeling, heat exchange, and nuclear waste disposal.[1] In a porous medium, the pores can be filled with fluids, and these fluids may have rheological properties, which open new possibilities to practical applications, such as thermal convection.[1,2] The effects of fluid relaxation and retardation on the convection dynamics in an Oldroyd viscoelastic fluid-saturated porous media have been studied by Sheu *et al.*[3] showing that the stress relaxation tends to accelerate the onset of chaos. These results were an extension of porous media of the work of Khayat and co-workers on nonlinear convection in viscoelastic fluids.[4–8] The aforementioned nonlinear studies were motived by the experimental works of Kolonder that found oscillatory instability on viscoelastic carrier liquids.[9] Subsequent work on a generalized model for viscoelastic fluids was performed by Pleiner *et al.*[10] Also, the thermal instability of an Oldroyd viscoelastic fluid in the presence of uniform rotation and suspended particles in hydromagnetics flow through a porous medium has been explored by Sharma and Sunil.[11,12] Pérez *et al.*[13,14] and Laroze and Pleiner[15] also considered the influences of the viscoelasticity on the thermal convection thresholds in an Oldroyd viscoelastic magnetic fluid heated from below. Furthermore, the investigation of chaotic and oscillatory magneto-convection in a binary viscoelastic fluid under g-jitter has been done by Bhadauria and Kiran[16] using a complex non-autonomous

Published under license by AIP Publishing.

Ginzburg–Landau equation. A stabilizing effect of the magnetic field, as it reduces both heat and mass transport, was found. Later, Bhadauria also investigated the effect of an internal heat source on the convection dynamics in a viscoelastic fluid-saturated porous medium.[17]

Since the early 1990s, the problem of controlling chaos has been considered among researchers and the scientific community. Poincaré's map linearization method (OGY method)[18] was the first chaos control free-model that established that the most significant changes on the chaotic behavior of non-linear dynamical systems produced by a very small deviation of its parameters were indeed unpredictable. Time-delayed feedback control has been suggested afterward by Pyragas,[19,20] showing that it could be employed in order to stabilize the chaotic system. Subsequently, Yau and Chen[21] showed that the Lorenz chaos could also be stabilized using a controller with input saturation, even when external system interference exists. In order to stabilize a dynamical system of unstable periodic orbits, Bessa *et al.* proposed a robust controller and found that chaos control can be done even in situations with some ambiguities.[22] Furthermore, after implementing the feedback control strategy, an amount of controller gain proportional to the scaled Rayleigh number[23–25] was found. Recently, the stability enhancement of a high Prandtl number chaotic convection has been studied for an anisotropic porous layer with feedback control.[26] Finally, some other important results on convection in porous media with viscoelastic fluids[27–34] need to be mentioned.

The aim of the present study is to continue the investigation of the feedback control influence on convective instability, motivated by the works on the chaotic nature of rheological parameters.[3] We derive a low-dimensional model using the Galerkin truncated approximation to the governing equations for thermal convection in an Oldroyd viscoelastic fluid in a saturated porous medium subject to gravity and heated from below. The novelty of the present paper is the combination of both the viscoelasticity and feedback control, which produce interesting convective states. In particular, we analyze the effect of the Rayleigh number, rheological parameters, as well as the feedback control on the dynamical behavior. We perform intensive numerical simulations to calculate two-dimensional diagrams of Lyapunov exponents as well as isospike diagrams. These diagrams distinguish the chaotic and regular regions in the parameter space. In particular, the thresholds of chaos as a function of the feedback control for several situations have been numerically computed. Furthermore, some notable topological structures in the regular states with a shape of *shrimps*[35,36] have been identified. In Sec. II, the model is presented and the generalized Lorenz equations are derived. In Sec. III, the numerical results are calculated and analyzed. Finally, in Sec. IV, the final remarks are given.

II. CONVECTION MODEL

An Oldroyd viscoelastic fluid in a saturated porous medium of height H_* and width L_* heated from below and cooled from above has been considered. The schematic setup is shown in Fig. 1. A Cartesian co-ordinate system is chosen making the vertical axis y collinear with gravity; i.e., $\vec{g} = -g\hat{e}_y$. The sensors and actuators are placed at the top and bottom heated plates of the fluid-saturated porous layer, respectively, as proposed by Tang and Bau.[37] The

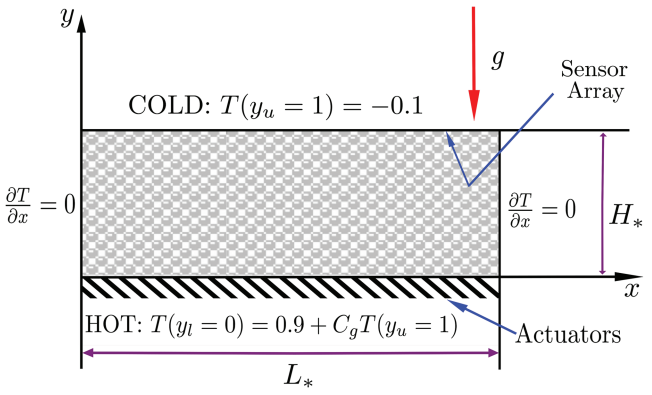


FIG. 1. Oldroyd viscoelastic fluid in a saturated porous medium of height H_* and width L_* heated from below and cooled from above.

determination and control, $\widehat{q}(t)$, were carried out by Bau[38] using the proportional–integral–differential (PID) controller,

$$\widehat{q}(t) = \mathscr{A} + C_g[e(t)], \tag{1}$$

where $\mathscr{A}$ is the calibration of the control and $e(t) = \widehat{m}(t) - m(t)$ is an error or the deviation from the state measurement $\widehat{m}(t)$ from some desired or reference value, $m(t)$. Also, the operator C_g is given by $C_g[f(t)] = C_p + C_D df/dt + C_I \int_0^t f(t')dt'$ where C_p is the proportional gain, C_D the differential gain, and C_I the integral gain. Based on Eq. (1), for one sensor plane and feedback control, the actuator regulates the heated surface temperature using a proportional linkage between the upper ($y = y_u$) and lower ($y = y_l$) thermal boundaries for the perturbation field; thus,

$$\theta(x, y_l, t) - \theta(x, y_l) = 0.9 + C_g[\theta(x, y_u, t) - \theta(x, y_u)] \tag{2}$$

or, homogeneously,[24]

$$\theta'(x, y_l, t) = 0.9 + C_g\theta'(x, y_u, t), \tag{3}$$

where θ' indicates the diversion of the fluid's temperature from its conductivity value and C_g is the scalar gain controller. The extended-Darcy model, including the time derivative, has been employed on the momentum equation to take the effect of the Prandtl number and viscoelasticity in a porous medium into consideration. The governing equations in the Boussinesq approximation are given by

$$\nabla \cdot \vec{q} = 0, \tag{4}$$

$$\left(1 + \zeta_1 \frac{\partial}{\partial t}\right)\left(\frac{\rho_R}{\varepsilon}\frac{\partial \vec{q}}{\partial t} + \nabla P - \rho\vec{g}\right) + \frac{\mu}{K}\left(1 + \zeta_2 \frac{\partial}{\partial t}\right)\vec{q} = 0, \tag{5}$$

$$\frac{\partial T}{\partial t} + \vec{q} \cdot \nabla T = \frac{1}{\alpha}\nabla^2 T, \tag{6}$$

where $\vec{q} = u\hat{e}_x + v\hat{e}_y$ is the fluid velocity field, P the fluid pressure, μ the fluid viscosity, K the permeability of the porous domain, ε the porosity, ρ the density, and T the temperature. Here, ζ_1 and ζ_2 denote the non-dimensional relaxation and retardation time, respectively. Also, the state equation for the density is

Published under license by AIP Publishing.

$\rho = \rho_R [1 - \beta (T - T_R)]$, where ρ_R is the reference density and β the coefficient of volume expansion. We remark that similar governing equations have been studied for other contexts in Refs. 39 and 40.

For a two-dimensional spatial system, the governing differential equations can be written in terms of a stream function defined by $u = -\partial\psi/\partial y$ and $v = \partial\psi/\partial x$, as for convective rolls having axis-aligned that refers to the shorter dimension (i.e., z) when $w = 0$. Implementing the curl ($\nabla\times$) operator on Eq. (5) yields the following equations:

$$\left[\frac{1}{Va}\left(1+\zeta_1\frac{\partial}{\partial t}\right)\frac{\partial}{\partial t}+\left(1+\zeta_2\frac{\partial}{\partial t}\right)\right]\nabla_\perp^2\psi = Ra\frac{\partial T}{\partial x} + Ra\zeta_1\frac{\partial^2 T}{\partial x\partial t}, \quad (7)$$

$$\frac{\partial T}{\partial t}-\frac{\partial\psi}{\partial y}\frac{\partial T}{\partial x}+\frac{\partial\psi}{\partial x}\frac{\partial T}{\partial y} = \nabla_\perp^2 T, \quad (8)$$

where $Va = \varepsilon Pr/Da$ is the Vadasz number, $Da = K/H_*^2$ is the Darcy number, and $Pr = \mu/\rho\kappa$ is the Prandtl number. Also, Ra is the Darcy–Rayleigh number defined as $Ra = \rho_0 g\beta(\Delta T)H_* K/\varepsilon\mu\kappa$. The Vadasz number represents the effect of porosity on flow in a porous media, and the Darcy–Rayleigh number accounts the ratio of buoyancy force to diffusive resistance of the porous media, which is also called the Rayleigh number for a porous medium.[23] The coordinates are dimensionless, and the horizontal Laplacian operator is given by $\nabla_\perp^2\psi = \partial^2\psi/\partial x^2 + \partial^2\psi/\partial y^2$.

Note that the set of partial differential equations (7) and (8) forms a nonlinear coupled system with boundary conditions. Ideal boundary conditions for the stream function $\psi = 0$ at $x = 0$ and $x = L$ as well as at $y = 0$ and $y = 1$ are used here. For the temperature field, $T(y = 1) = -0.1$ and $T(y = 0) = 0.9 + C_g T(y = 1)$, while $\partial T/\partial x = 0$ at $x = 0$ and $x = L$ is imposed. Note that, for an uncontrolled limit ($C_g \to 0$), these are reduced to $T(y = 1) = -0.1$ and $T(y = 0) = 0.9$. Similar types of boundary conditions have been employed in other convection in porous media problems.[23,41,42] In Sec. II A, we will use a Galerkin method to analyze the system.

A. Generalized Lorenz system

The Fourier spectral method is used to obtain the solution of the nonlinear coupled system of partial differential equations (7) and (8). A truncated Galerkin expansion of the Lorenz-similar form[43,44] is used. For this purpose, the lateral direction will be restricted to the fundamental mode, neglecting higher harmonics in the x-direction. This assumption can be made when considering a large container. On the y-direction across the layer, a multimode description will be used when necessary. Higher harmonics describe deviations of the variables from the linear regime, thus representing the stream and the temperature function in the respective forms,

$$\psi(t,x,y) = A_{11}(t)\sin\left(\frac{\pi x}{L}\right)\sin(\pi y), \quad (9)$$

$$T(t,x,y) = T_0(y) + B_{11}(t)\cos\left(\frac{\pi x}{L}\right)\sin(\pi y) + B_{02}(t)\sin(2\pi y), \quad (10)$$

where $T_0(y) = (1/10)\left[9 - C_g - (10 - C_g)y\right]$. Similar to the Lorenz model, we analyze the effect of second harmonics only in the temperature.[43] Then, substituting Eqs. (9) and (10) into Eqs. (7) and (8) and considering the orthogonal characteristic functions corresponding to Eqs. (9) and (10), we get a set of ordinary differential equations for the time evolution of the amplitudes integrating them over the spatial domain,

$$\left[\left(1+\Gamma\frac{d}{d\tau}\right)\frac{d}{d\tau}+\varepsilon\left(1+\Gamma\Lambda\frac{d}{d\tau}\right)\right]A_{11} = \frac{\varepsilon Ra}{\chi\pi}\left(1+\Gamma\frac{d}{d\tau}\right)B_{11},$$

$$\frac{dB_{11}}{d\tau} = -B_{11} + \frac{10 - C_g}{10\pi\chi}A_{11} + \frac{1}{\chi}A_{11}B_{02},$$

$$\frac{dB_{02}}{d\tau} = -\frac{1}{2\chi}A_{11}B_{11} - 4\gamma B_{02},$$

where $\tau = \pi^2 t/\gamma$, $\sigma = Va\gamma/\pi^2$, and $\chi = 1/(L\gamma)$ such that $\gamma = L^2/(L^2+1)$. Note that γ is a geometric parameter. Here, $\Lambda = \zeta_2/\zeta_1$ is the retardation number and $\Gamma = \zeta_1\pi^2/\gamma$ is the Deborah number. These two dimensionless numbers account for the viscoelastic properties of the fluid. Usually, the Deborah number measures the strength of the viscoelasticity, and the retardation number estimates the delayed response of the fluid under a force.[4] Rescaling the amplitudes in the form $X = A_{11}/\left(2\chi\sqrt{2\gamma\left(\overline{C}_g r - 1\right)}\right)$, $Y = \pi r B_{11}/\left(2\sqrt{2\gamma\left(\overline{C}_g r - 1\right)}\right)$, and $Z = -\pi r B_{02}/\left(\overline{C}_g r - 1\right)$, the following set of equations is obtained:

$$\dot{X} = W, \quad (11)$$

$$\dot{Y} = \overline{C}_g r X - Y - \left(\overline{C}_g r - 1\right)XZ, \quad (12)$$

$$\dot{Z} = 4\gamma(XY - Z), \quad (13)$$

$$\dot{W} = \sigma\left[\left(\overline{C}_g r - \frac{1}{\Gamma}\right)X + \overline{\Gamma}Y - \left(\overline{C}_g r - 1\right)XZ - \overline{\Lambda}W\right], \quad (14)$$

where the dot $(\cdot)$ denotes the time derivative $\mathrm{d}()/\mathrm{d}\tau$. Here, for convenience, the following notation $r = Ra/\pi^2\chi^2$, $\overline{C}_g = (10 - C_g)/10)$, $\overline{\Lambda} = (\Lambda + (\sigma\Gamma)^{-1})$, and $\overline{\Gamma} = -1 + 1/\Gamma$ is introduced. The aforementioned 4D dynamical systems is a generalization of the Lorenz equations, $\dot{\mathbf{X}} = \mathbf{F(X)}$, which takes into account the viscoelastic effects as well as the feedback control.

Of course, when $C_g = 0$, the uncontrolled case[3] is recovered,

$$\dot{X} = W, \quad (15)$$

$$\dot{Y} = rX - Y - (r-1)XZ, \quad (16)$$

$$\dot{Z} = 4\gamma(XY - Z), \quad (17)$$

Published under license by AIP Publishing.

$$\dot{W} = \sigma\left[\left(r - \frac{1}{\Gamma}\right)X + \overline{\Gamma}Y - (r-1)XZ - \overline{\Lambda}W\right], \tag{18}$$

which itself is the complement for the porous medium of the work of Khayat and co-workers on convention in viscoelastic fluids.[4–8] The Newtonian limit requires that the viscoelastic parameters take the following limits $\Gamma \to 0$ and $\Lambda \to 1$. In this case, Eq. (14) is transformed into an algebraic equation, $W \to \sigma(Y - X)$. Consequently, the system (11)–(14) is reduced to

$$\dot{X} = \sigma(Y - X), \tag{19}$$

$$\dot{Y} = \overline{C}_g r X - Y - \left(\overline{C}_g r - 1\right)XZ, \tag{20}$$

$$\dot{Z} = 4\gamma(XY - Z). \tag{21}$$

This modified Lorenz system was studied in Refs. 25 and 26. It is clear that the effect of viscoelasticity adds an extra dimension to the system. Let us also comment that there is an elegant form to derive the viscoelastic effects on the Lorenz system using an independent field for the viscoelastic terms. More details can be found in Refs. 45 and 46.

On the other hand, the stationary solutions of the system ($\dot{\mathbf{X}} = \mathbf{0}$) are $(X_0, Y_0, Z_0, W_0) = (0, 0, 0, 0)$ that represents the conduction state and $(X_\pm, Y_\pm, Z_\pm, W_\pm) = (\pm 1, \pm 1, 1, 0)$ that corresponds to the onset of convective rolls. To analyze the stability of each stationary solution, $\mathbf{X}_S$, let us suppose that $\mathbf{X}(\tau) = \mathbf{X}_S + \delta\mathbf{X}(\tau)$, where $\delta\mathbf{X}(\tau)$ is a perturbation such that $|\delta\mathbf{X}| \ll 1$. The linearized equation around $\mathbf{X}_S$ is $\delta\dot{\mathbf{X}} = \overline{\mathbf{J}} \cdot \delta\mathbf{X}$, where $\overline{\mathbf{J}}$ is the Jacobian matrix. In our problem, $\overline{\mathbf{J}}$ can be written as

$$\overline{\mathbf{J}} = \begin{pmatrix} 0 & 0 & 0 & 1 \\ r\overline{C}_g - \left(r\overline{C}_g - 1\right)Z_S & -1 & \left(1 - r\overline{C}_g\right)X_S & 0 \\ 4\gamma Y_S & 4\gamma X_S & -4\gamma & 0 \\ \sigma\left(1 - r\overline{C}_g\right)Z_S + \sigma\left(r\overline{C}_g - \dfrac{1}{\Gamma}\right) & \sigma\left(\dfrac{1}{\Gamma} - 1\right) & \sigma\left(1 - r\overline{C}_g\right)X_S & -\sigma\left(\Lambda + \dfrac{1}{\Gamma\sigma}\right) \end{pmatrix}. \tag{22}$$

The associated eigenvalue problem $\delta\dot{\mathbf{X}} = s\delta\mathbf{X}$ produces the secular equation

$$b_0 + b_1 s + b_2 s^2 + b_3 s^3 + b_4 s^4 = 0, \tag{23}$$

where the coefficients b_j with $j = (0, \ldots, 4)$ are explicitly given in the Appendix. Let us focus on the stationary solution for the onset of convective rolls. Its Hopf bifurcation is produced when $s = i\omega$, such that $\omega \in \Re$. Therefore, in this case, Eq. (23) is split into its real and imaginary parts,

$$b_0 - b_2\omega^2 + b_4\omega^4 = 0, \tag{24}$$

$$b_1\omega - b_3\omega^3 = 0. \tag{25}$$

Solving these coupled equations, the marginal curves for the critical values of the control parameter as well as the critical frequency ω for the Hopf bifurcation can be obtained. Usually, these equations are used to obtain the critical Rayleigh number, r_H, when the other parameter are fixed, but it can also be used to compute the critical Deborah number, Γ_H, when r and the rest of the parameters are fixed. In both cases, the subindex H has been employed to denote the type of bifurcation. Finally, notice that Eq. (25) provides two kinds of solutions: the first solution is $\omega = 0$ and the second one is $\omega^2 = b_1/b_3$ if and only if $b_3 \neq 0$. In the following, we will be interested in the second case, $\omega \neq 0$.

In Sec. III, full numerical simulations of this generalized Lorenz system will be performed, including comparisons with the linear stability analysis and the Newtonian limit as well.

III. NUMERICAL RESULTS

In this section, the behavior of the system (11)–(14) as a function of the parameters is examined using Lyapunov exponents, bifurcation diagrams, and direct time-series analysis, like the Fast Fourier Transform (FFT). The bifurcation diagrams are computed by counting the values of the local maximum of the time series of a specific variable.[44] For a N-dimensional dynamical system, the Lyapunov exponents measure the sensibility of the initial conditions.[47,48] They are commonly denoted by the symbols λ_j with $j = (1, \ldots, N)$ and ordered in a decreasing form, such as the largest Lyapunov exponent (LLE), denoted by λ_1. The exponential divergence of two initially close trajectories, which is characteristic for chaotic dynamics, is detected when positive LLE is found. If the LLE is negative, the state is stationary, whereas when LLE is zero, the system exhibits a regular state, which can be periodic or quasiperiodic. Besides, if there are two positive Lyapunov exponents, the system exhibits a hyper-chaotic state.[49–51] If both the largest and the second largest Lyapunov exponents are zero, the system holds a quasiperiodic state. This technique has been well established in several dynamical systems.[48,52–54] The numerical method to solve the equations is the classical fourth order Runge–Kutta method with a fixed time step of $\Delta\tau = 5 \times 10^{-3}$. Other values of $\Delta\tau$ have been employed to check the accuracy, yielding no significant changes. Due to the large numbers of parameters, $\gamma = 0.5$ and $\sigma = 100$ will be fixed. Parameters r, C_g, Γ as well as Λ will be varied in order to characterize the effect of the external driven temperature, the feedback control, and the viscoelasticity. Intensive numerical simulations are performed. In several cases, two parameters are simultaneously varied, creating two-dimensional phase diagrams of different dynamical indicators.

Published under license by AIP Publishing.

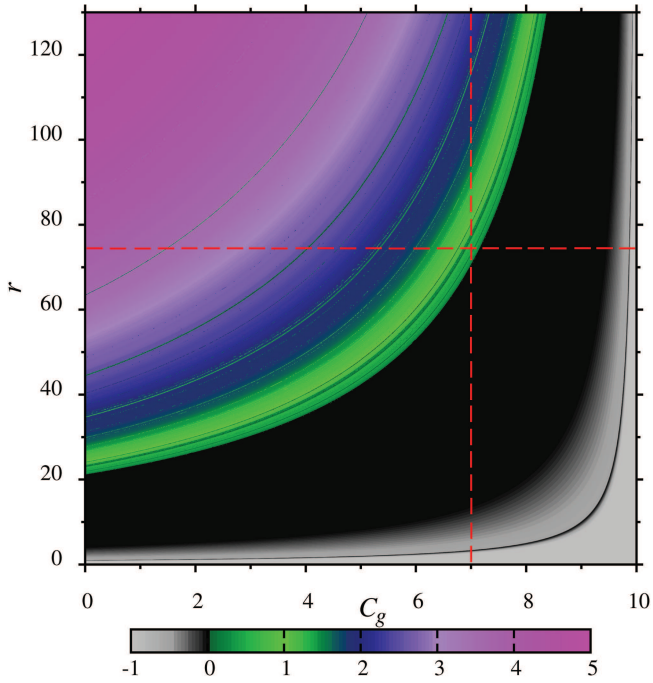


FIG. 2. Phase diagram in a color code of the largest Lyapunov exponent (LLE) as a function of the Rayleigh number r and the feedback control parameter C_g. The fixed parameters are $\Gamma = 1.0$, $\Lambda = 0.2$, $\sigma = 100$, and $\gamma = 0.5$. The vertical and horizontal dashed lines represent cuts at $C_g = 7.0$ and $r = 75$, respectively.

The resolution of each diagram is 2000×2000 in the parameter space.

A. Thermal and feedback control effects

Figure 2 displays a phase diagram in a color code of LLE as a function of the Rayleigh number, r, and the feedback control parameter, C_g. For small values of r, and until $r \gtrsim 20$, the system exhibits only regular behavior. This value increases with C_g. We can recognize that several transitions from chaotic to regular states are revealed in the diagram. These transitions decrease when r increases under low and intermediate values of C_g. Note that the chaotic domains are bounded in the $r - C_g$ plane. Hence, we can infer that C_g can be used to suppress chaos and, consequently, to induce stationary as well as periodic states. Let us study with detail the effect of each parameter. For this purpose, we will analyze a vertical as well as a horizontal cut in the phase diagram at $C_g = 7.0$ and $r = 75$, respectively.

The upper panel of Fig. 3 shows the LLE and the corresponding bifurcation diagram for the Z-component as a function of the reduced Rayleigh number, r. We can observe that for values approximately within the range $r \lesssim 13.8$, the system presents stationary solutions, while for values approximately between $r \in (13.8, 70.6)$, the solutions are regular ($\lambda_1 = 0$). However, when $r \gtrsim 70.7$, the system bifurcates into chaotic states. After this value, the transitions between regular and chaotic states are recurrent with periodic

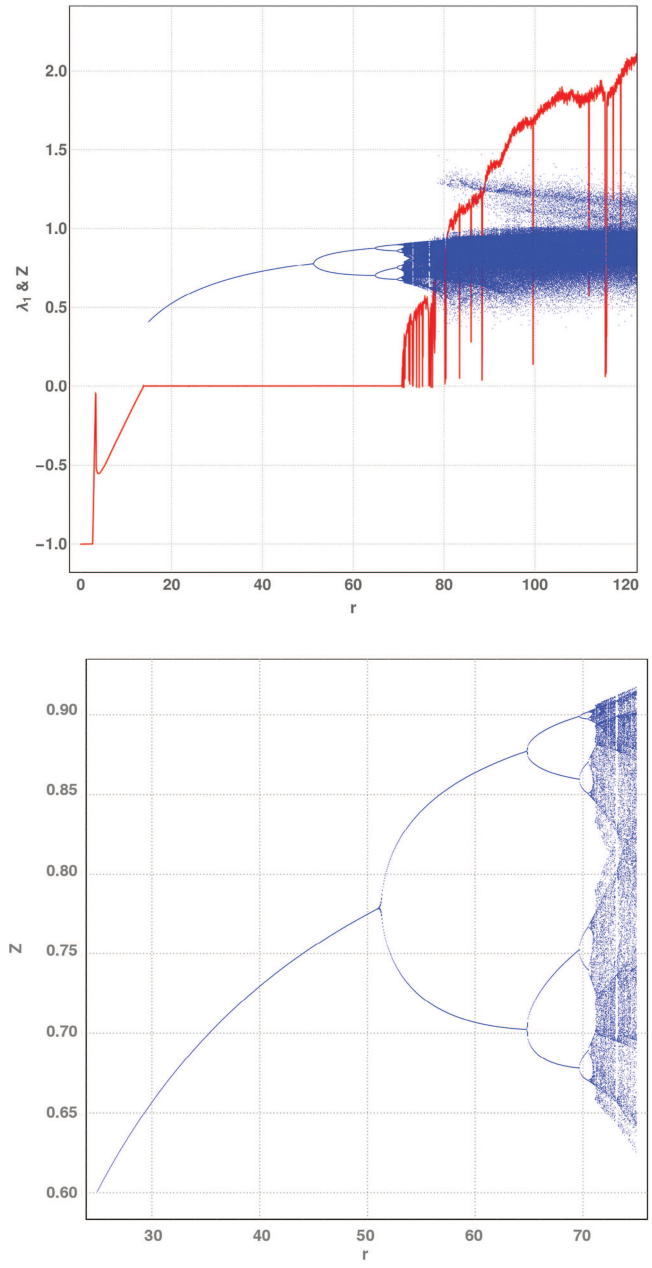


FIG. 3. Largest Lyapunov exponent (LLE) and the bifurcation diagram as a function of the reduced Rayleigh number r at $C_g = 7.0$. The lower panel shows a zoom of the bifurcation diagram for $r \in (20, 80)$. The other fixed parameters are $\Gamma = 1.0$, $\Lambda = 0.2$, $\sigma = 100$, and $\gamma = 0.5$. This figure is indicated with the vertical dashed line of Fig. 2.

islands inside chaotic windows. This phenomenon of periodic windows is similar to the observed in viscoelastic systems[8,15,55] as well as in other complex fluids.[56,57] For a deeper insight, in the lower panel of Fig. 3, a more accuracy zoom of the bifurcation diagram within

Published under license by AIP Publishing.

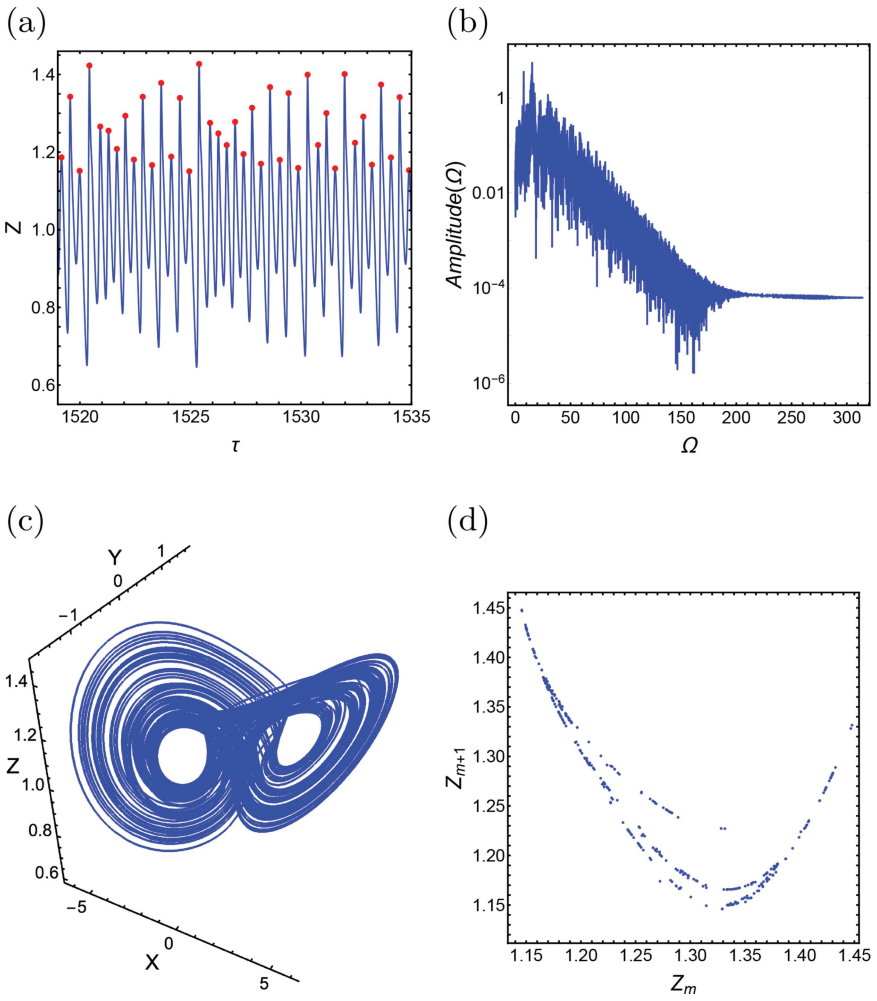


FIG. 4. (a) Time series of the Z-component. (b) Amplitude of the fast Fourier transform (FFT) as a function of the frequency for the Z-component. (c) 3D parametric plot of (X, Y, Z). (d) Recurrence plot of the local maximum Z_{m+1} as a function of the local maximum Z_m. Here, $r = 75$ and the other fixed parameters are the same as in Fig. 3.

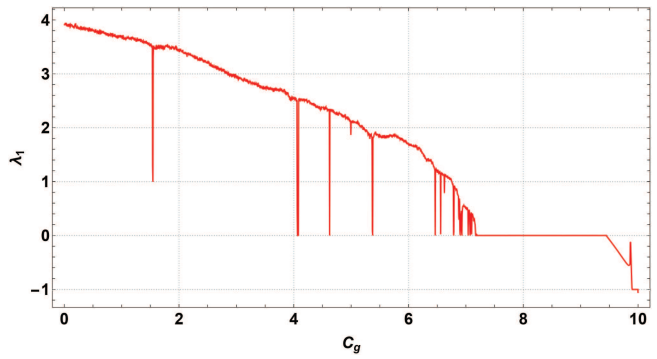


FIG. 5. LLE as a function of the feedback control parameter C_g at $r = 75$. The other fixed parameters are $\Gamma = 1.0$, $\Lambda = 0.2$, $\sigma = 100$, and $\gamma = 0.5$. This figure is indicated with the horizontal dashed line of Fig. 2.

the range $r \in (20, 80)$ is computed. Well-defined doubling period cascades become visible until the system bifurcates to chaotic states.

In Fig. 4, we study an example of a chaotic state for $r = 75$ with the same fixed parameters as in Fig. 3. The panel (a) shows the time series of the Z-component of the system, where an irregular behavior can be observed. The panel (b) corresponds to the FFT of the Z component, $A(\Omega)$, as a function of the frequency Ω. It shows as a continuum of frequencies, which is typical for chaotic states. The 3D parametric plot of components (X, Y, Z) shows a butterfly form, similar to that of the Lorenz attractor.[44] Finally, panel (d) shows a recurrence diagram for the local maxima Z_{M+1} as a function of Z_M. Apart from the Lorenz recurrent relation, this one is more complex due to the extra dimension of the dynamical system.

Figure 5 shows the LLE as a function of the feedback control parameter C_g for a high value reduced Rayleigh number, $r = 75$. For small values of C_g, the system mostly exhibits chaotic behavior with the exception of a few periodic islands. Within the approximated range $C_g \in (7.2, 9.45)$, the system presents regular states, whereas for higher values, $C_g \gtrsim 9.45$, the solutions become stationary. Two different non-chaotic states as a function of the value of C_g taken

Published under license by AIP Publishing.

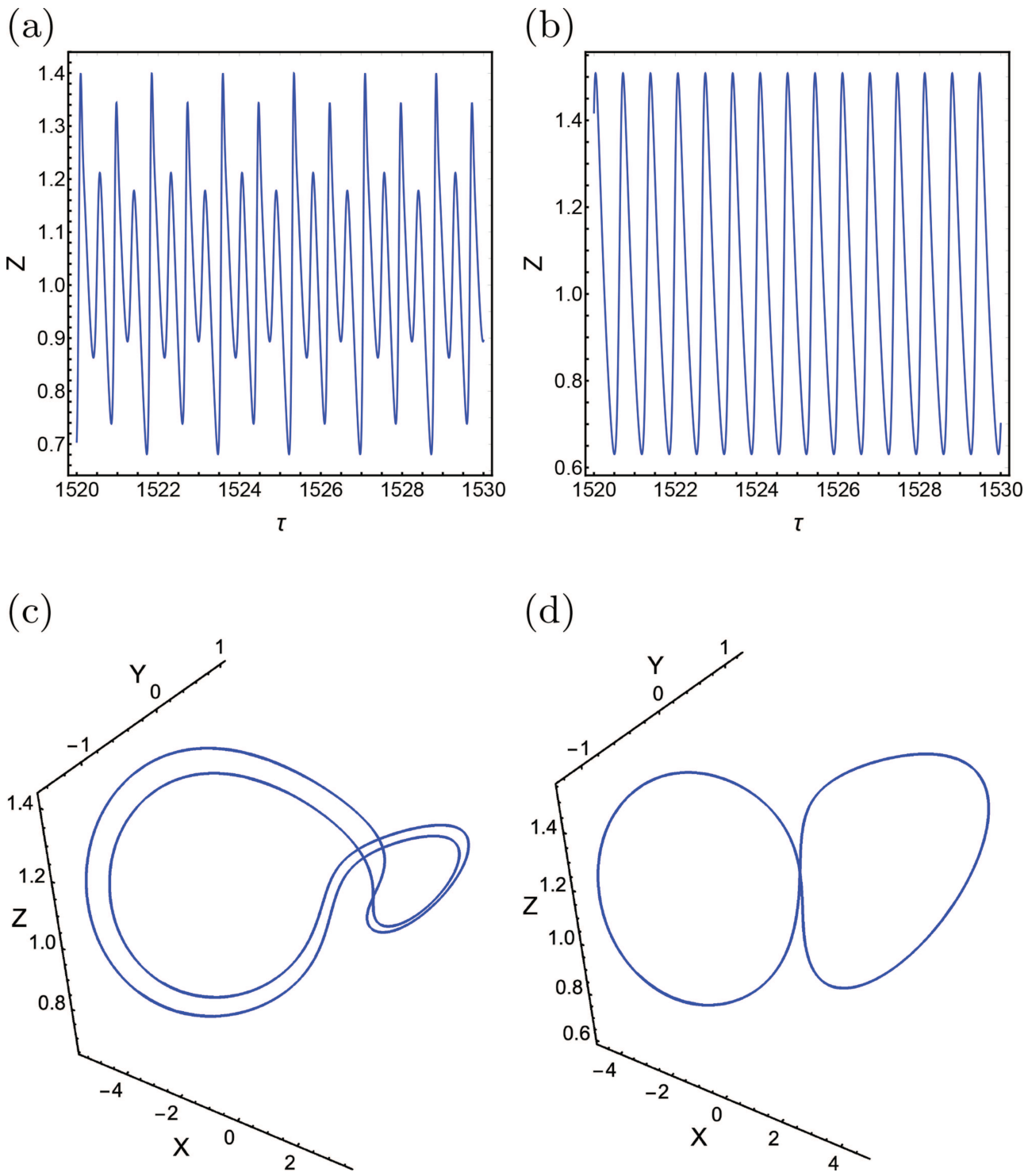


FIG. 6. Temporal series and the phase space of different states as a function of the feedback control parameter C_g with two periodic states. Panels (a) and (c) show states at $C_g = 7.3$, while panels (*b*, *d*) show states at $C_g = 8.9$. The remaining fixed parameters are as in Fig. 5.

Published under license by AIP Publishing.

from the LLE diagram given in Fig. 5 require further analysis. The temporal series of the Z-component and the corresponding 3D parametric plot of (X, Y, Z) are shown in Fig. 6. These two cases are regular with two different types of periodicity, as can be observed in the 3D parametric plots. The values of the LLE below $\lambda_1 \sim 10^{-4}$ are considered as a numerical zero.

Several types of periodic solutions can be found in the generalized Lorenz system. An appropriate manner to study them is using the isospike technique.[36,58–60] This method measures the number of spikes per period of the oscillations. This kind of diagram reveals in detail the periodic states of the system.[36] To calculate them, we first calculate the LLE and perform the integrations for 3×10^5 time steps, recording the maxima (or minima) of the time series and checking whether the peaks are repeated or not. Figure 7 displays the phase diagram in a color code of the isospike diagram of the Z-component as a function of the Rayleigh number r and the feedback control parameter C_g. Here, a palette of 16 colors has been used to represent the number of peaks contained in a period of oscillations, as indicated by the color bars in the aforementioned figure. States with more than 16 peaks are drawn in gray. White represents the stationary states, while black is for chaotic ones. We can observe that for small values of the reduced Rayleigh number, stationary states are found. Later, the system suffers a Hopf bifurcation. The curve for the critical Rayleigh number at this bifurcation,

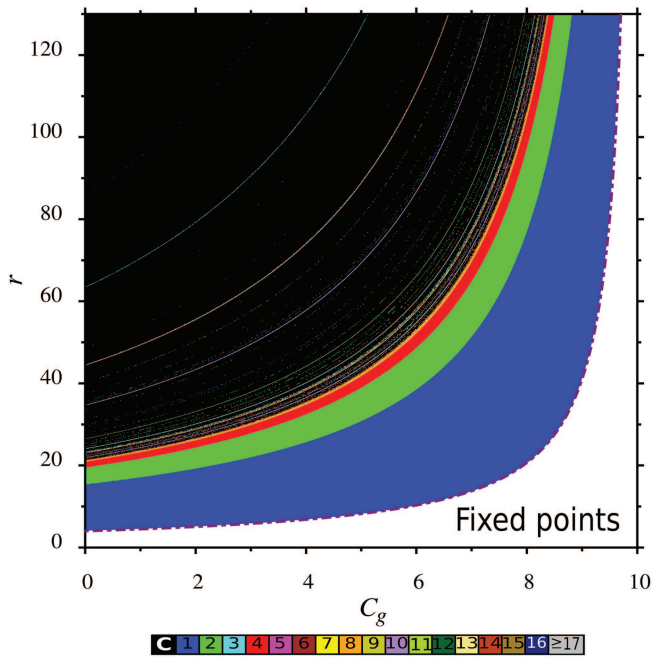


FIG. 7. Phase diagram in a color code of the isospike diagram of the Z-component as a function of the Rayleigh number r and the feedback control parameter C_g. The fixed parameters are $\Gamma = 1.0$, $\Lambda = 0.2$, $\sigma = 100$, and $\gamma = 0.5$. The resolutions are $\Delta r = 0.06$ and $\Delta C_g = 0.005$. The dashed–dotted curve represents the critical Rayleigh number r_H as a function of C_g, obtained from the linear stability analysis.

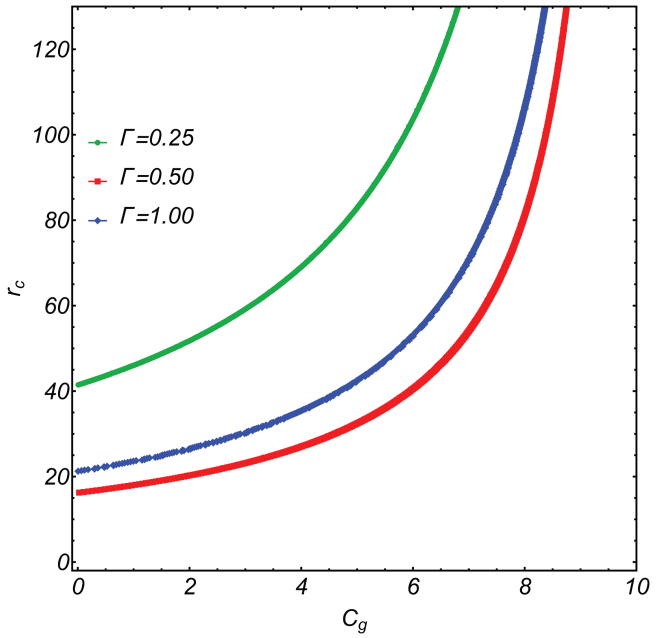


FIG. 8. Critical reduced Rayleigh number r_c as a function of the feedback control parameter C_g for different values of Γ. The fixed parameters are $\sigma = 100$, $\Lambda = 0.2$, and $\gamma = 0.5$.

TABLE I. Fitting parameters for r_c.

Γ	r_{c0}	ε_1	η_1	ε_2	η_2
0.25	41.470	4.242	1.283	1.95×10^{-3}	5.154
0.50	16.250	0.644	2.021	8.45×10^{-10}	11.527
1.00	21.255	1.289	1.739	2.28×10^{-7}	9.096

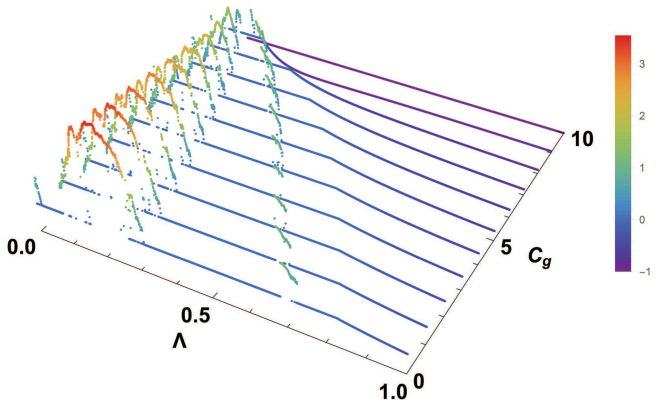


FIG. 9. 3D diagram in a color code of LLE as a function of the retardation number Λ and the feedback control parameter C_g. The fixed parameters are $r = 75$, $\Gamma = 0.5$, $\sigma = 100$, and $\gamma = 0.5$.

Published under license by AIP Publishing.

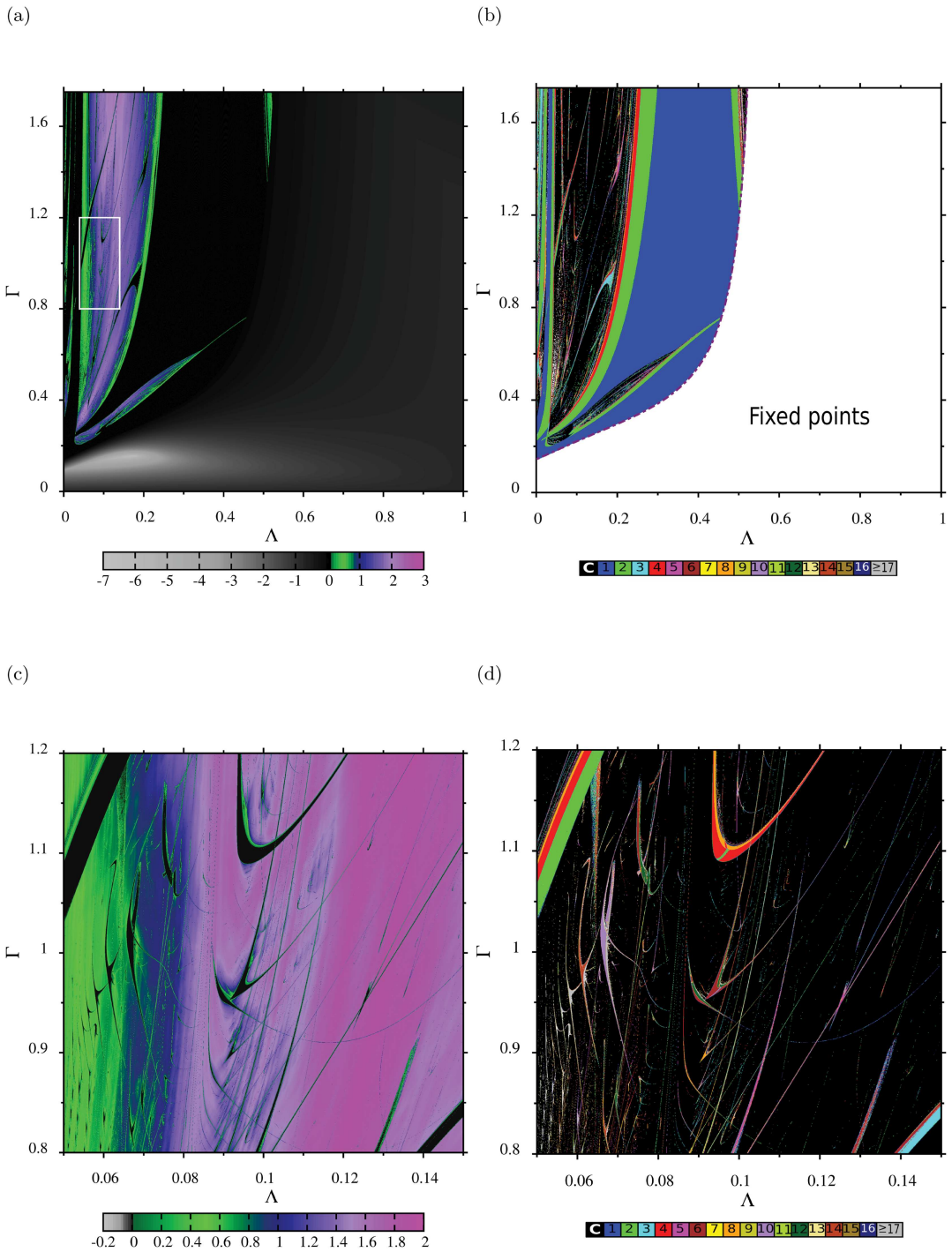


FIG. 10. (Top) Phase diagrams in a color code of the LLE (a) and isospike (b) as a function of both viscoelastic parameters Γ and Λ. The resolutions are $\Delta\Gamma$ and $\Delta\Lambda = 0.01$. (Bottom) Zoom of both diagrams in the region is indicated with a white box of panel (a). Here, the new resolutions are $\Delta\Gamma$ and $\Delta\Lambda = 0.01$. The fixed parameters are $r = 75$, $C_g = 7.0$, $\sigma = 100$, and $\gamma = 0.5$. In panel (b), the dashed–dotted curve represents the critical Deborah number Γ_H as a function of Λ, obtaining from the linear stability analysis.

Published under license by AIP Publishing.

$r_H = r_H(C_g)$, is computed from the resulting equations of the linear analysis [Eqs. (24) and (25)]. Subsequent transitions to more complex periodic solutions appear symmetrically in the $C_g - r$ plane. In particular, bands of periodic domains emerge one after the other, such that the first bifurcations are through period doubling: $1 \to 2 \to 4 \to 8$, which is in agreement with the bifurcation diagram displayed in Fig. 3. After the first transition to chaos, the periodic states are presented in small bands on the $C_g - r$ plane in a somewhat disordered fashion. Some of the lines have the same periodicity, but in others, there is a fragmentation of multiple periodicities, even with higher spike values. Moreover, for higher values of r and small and intermediate values of C_g, the occurrence of periodic states decreases, and the bands become lines. The periodicities of these lines are concentrated in more defined values of spikes. For large values of C_g, there are only regular states, and chaos is totally suppressed. In fact, when C_g increases, all the states become stationary ones.

1. Suppression of chaos

In order to explore how robust is the suppression of chaos in Fig. 8, the critical reduced Rayleigh number r_c is shown as a function of the feedback control parameter C_g for different values of the Deborah number Γ. Under this critical value, chaotic states are suppressed. These thresholds have been calculated using the information of two-dimensional diagrams of the LLE as a function of both r and C_g (with a resolution of 2000×2000 in the space parameter). The corresponding LLE diagrams at $\Gamma = (0.25, 0.5, 0.75)$ are displayed in the supplementary material. We observe that r_c increases smoothly with C_g. In fact, we can numerically infer that the critical reduced Rayleigh number follows the law,

$$r_c \approx r_{c0} + \varepsilon_1 C_g^{\eta_1} + \varepsilon_2 C_g^{\eta_2}, \tag{26}$$

where $(r_{c0}, \varepsilon_j, \eta_j)$ are fitting parameters that depend on the Deborah number. Notice that the effect of Γ on r_c produces an alteration on its initial value of r_{c0} but only slight changes in the exponents η_1. For the three values of Γ, we found that $\eta_2 > \eta_1$ and that $\varepsilon_2 \ll 1$, giving a correction to the principal power law. All fitting data are given in Table I.

Figure 9 shows a three-dimensional diagram in a color code of LLE as a function of the retardation number Λ and the feedback control parameter C_g. In the uncontrolled case $C_g = 0$, the range of chaotic regions is more significant than in the controlled one. Note that for $C_g = 10$, only stationary solutions can be found because the LLE is lower than zero for all values of Λ. Furthermore, we remark that the critical retardation number, Λ_c, in which the chaotic states are suppressed above this value follows an approximately linear relationship, $\Lambda_c \approx 0.729 - 0.068 C_g$. We can infer that both parameters accelerate the suppression of chaos.

B. Viscoelastic effects

Let us now analyze in more detail the effect in the viscoelasticity. Figure 10 shows phase diagrams in a color bar code of the LLE and the isospike diagram of the Z-component as a function of both viscoelastic parameters Γ and Λ. The same color code of the previous diagrams is used here. The top panels show a wider range of the parameters, while the bottom ones are the corresponding iterative zooms demarcated in the white box of panel (a). We can observe that the chaotic regions can be found from values of $\Lambda \lesssim 0.51$. The global curve that separates the mixed areas from pure stationary solutions is $\Gamma_H = \Gamma_H(\Lambda)$, which is computed by the resulting equations of the linear analysis [Eqs. (24) and (25)]. This separatrix is denoted in panel (b). Above this curve, periodic and chaotic states coexist, such that the transitions among these regions are considerably complex. In fact, within chaotic state domains, well-defined topological structures of regular states are found. To see in more detail this type of structures, we perform a zoom in the region $\Delta\Gamma \otimes \Delta\Lambda = (0.8, 1.2) \otimes (0.05, 0.15)$ displayed in panels (c) and (d). Note that some structures with shapes such as shrimps and boomerangs appear. These structures have been studied in a wide spectrum of physical contexts.[53,58–60] As observed in panel (d), the shrimp periodicities are varied, and some of them are quite high. In addition, in the case of boomerangs, they have a combination of periodic areas centered on $(\Gamma, \Lambda) = (1.1, 0.1)$, where each upper branch has period four and is divided by a band of period two. Let us finally comment that the variety of complexity in these structures is rich. To illustrate this point, the supplementary material includes other LLE diagrams for a different set of fixed parameters.

C. Newtonian limit

Finally, let us investigate the Newtonian limit from the Lyapunov exponent's point of view. In this limiting case, the dynamical system is reduced to a three-dimensional one, given by Eqs. (19)–(21). This system has been previously studied using the direct time series analysis and bifurcation diagrams as a function of the reduced Rayleigh number, r, for a few values of the feedback control parameter, C_g. Also, the effect of the Valzald number, σ, has been examined. State-of-the-art can be found in Refs. 23, 25, and 26. Here, we perform a phase diagram of the LLE as a function of r and C_g at $\sigma = 100$. This result is displayed in panel (a) of Fig. 11. We can observe that chaotic regions appear for higher values of r and small and intermediate values of C_g. These regions have ring band shapes, alternated by a band of regular states. The

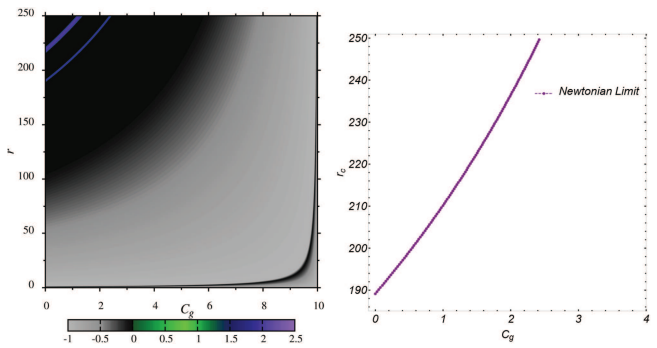


FIG. 11. (a) Phase diagram in a color code of LLE as a function of the Rayleigh number r and the feedback control parameter C_g in the Newtonian limit at $\sigma = 100$ and $\gamma = 0.5$. (b) The corresponding critical reduced Rayleigh number r_c as a function of the feedback control parameter C_g for different values of Γ.

Published under license by AIP Publishing.

panel (b) of Fig. 11 shows the critical reduced Rayleigh number, r_c. Below this value, the chaotic states are suppressed as a function of the feedback control parameter C_g. We can observe that r_c follows the same form of Eq. (26) with $r_{c0} = 189.13$, $\varepsilon_1 = 19.3633$, $\varepsilon_2 = 1.673\,58$, $\eta_1 = 1.0$, and $\eta_2 = 2.365\,92$. Note also that the range of C_g for the Newtonian case is narrow with respect to the viscoelastic case. Therefore, the influence of the feedback control is more substantial in the Newtonian limit.

IV. FINAL REMARKS

In this paper, the effects of feedback control and viscoelasticity on chaotic and periodic dynamics in the problem of thermal convection in an Oldroyd viscoelastic fluid in a saturated porous medium have been studied for a wide range of the Rayleigh number. The study has been based on the dynamical systems theory. In particular, using a truncated Galerkin expansion, a set of four coupled nonlinear differential equations has been derived. Using Lyapunov exponents and bifurcation diagrams, the following findings have been attained. For small values of the reduced Rayleigh number, the system presents stationary states. However, for values approximately between $r \in (13.8, 70.6)$, the solutions are regular. This new periodic window is completely different from the Lorenz model. This is clearly a consequence of the combined effect of the feedback control and the viscoelasticity. Furthermore, the effect of the feedback control produces a suppression of chaos in a wide range of parameters, as it is shown in Fig. 8. In fact, the critical reduced Rayleigh number in which the chaotic states are overcome follows a combination of power laws as a function of C_g. Hence, this control feedback method can be used for taming chaotic behaviors in convection. The effect of the viscoelasticity generates both periodic as well as chaotic windows with complex forms. Indeed, some well-known topological structures of regular domains,[35,59,60] such as shrimps and boomerangs, are found in the Γ–Λ parameter plane. The periodicity of these structures can be varied as was revealed in the isospike diagrams of Fig. 10. Finally, the effect of more modes in the Galerkin expansion[61] is indeed an appealing topic and will be studied in future works.

SUPPLEMENTARY MATERIAL

See the supplementary material for the complementary information concerning LLE phase diagrams as a function of C_g and r as well as LLE phase diagrams as a function of Γ and Λ. The corresponding sets of fixed parameters are different from those included in the main text.

ACKNOWLEDGMENTS

Our thanks to Ana Cabanas (Universidad de Tarapacá) and David Becerra-Alonso (Universidad Loyola Andalucía) for a critical reading of the manuscript. D.L. acknowledges the partial financial support from centers of excellence with BASAL/CONICYT (Grant No. AFB180001), CEDENNA. L.M.P. and D.L. acknowledge the partial financial support of FONDECYT (No. 1180905).

APPENDIX: COEFFICIENTS OF THE SECULAR EQUATION FOR THE LINEAR STABILITY ANALYSIS

The coefficients b_j with $j = (0, \ldots, 4)$ of the secular equation (23) are given by

$$b_0 = 4\gamma\sigma\left(r\overline{C}_g - 1\right)\left(X_S\left(X_S + Y_S\right) + Z_S - 1\right), \tag{A1}$$

$$b_1 = 4\gamma\left(\Gamma\Lambda\sigma + 1\right)\left(r\overline{C}_g - 1\right)X_S^2 + 4\gamma\Gamma\sigma\left(r\overline{C}_g - 1\right)X_S Y_S + \sigma\left(4\gamma\Gamma + 1\right)\left(r\left(Z_S - 1\right)\overline{C}_g - Z_S\right) + 4\gamma\left(\Gamma\Lambda\sigma + \sigma + 1\right) + \sigma, \tag{A2}$$

$$b_2 = 4\gamma\Gamma\left(r\overline{C}_g - 1\right)X_S^2 + \Gamma\sigma\left(r\left(Z_S - 1\right)\overline{C}_g - Z_S\right) + 4\gamma\left(\Gamma\Lambda\sigma + \Gamma + 1\right) + \Gamma\Lambda\sigma + \sigma + 1, \tag{A3}$$

$$b_3 = 4\gamma\Gamma + \Gamma\Lambda\sigma + \Gamma + 1, \tag{A4}$$

$$b_4 = \Gamma. \tag{A5}$$

Note that in the coefficients b_j, the terms with X_S and Y_S appear in a quadratic form: X_S^2 and $X_S Y_S$. Therefore, the sign on the stationary solutions for the onset of convective rolls $\mathbf{X}_S = (\pm 1, \pm 1, 1, 0)$ will not play a role in this analysis.

DATA AVAILABILITY

The data that support the findings of this study are available from the corresponding author upon reasonable request.

REFERENCES

[1] D. A. Nield and A. Bejan, *Convection in Porous Media*, 5th ed. (Springer International Publishing AG, Switzerland, 2017).
[2] J. Bear, *Modeling Phenomena of Flow and Transport in Porous Media* (Springer International Publishing AG, Switzerland, 2018).
[3] L. J. Sheu, L. M. Tam, J. H. Chen, H. K. Chen, K. T. Lin, and Y. Kang, "Chaotic convection of viscoelastic fluids in porous media," Chaos Solitons Fractals **37**, 113 (2008).
[4] R. E. Khayat, "Non-linear overstability in the thermal convection of viscoelastic fluids," J. Non-Newtonian Fluid Mech. **53**, 331 (1994).
[5] R. E. Khayat, "Chaos and overstability in the thermal convection of viscoelastic fluids," J. Non-Newtonian Fluid Mech. **53**, 227 (1995).
[6] R. E. Khayat, "Nonlinear overstability in the thermal convection of viscoelastic fluids," J. Non-Newtonian Fluid Mech. **58**, 331 (1995).
[7] R. E. Khayat, "Chaos in the thermal convection of weakly shear-thinning fluids," J. Non-Newtonian Fluid Mech. **63**, 153 (1996).
[8] E. Abu-Ramadan, J. M. Hay, and R. E. Khayat, "Characterization of chaotic thermal convection of viscoelastic fluids," J. Non-Newtonian Fluid Mech. **115**, 79 (2003).
[9] P. Kolodner, "Oscillatory convection in viscoelastic DNA suspensions," J. Non-Newtonian Fluid Mech. **75**, 167 (1998).
[10] H. Pleiner, M. Liu, and H. R. Brand, "Nonlinear fluid dynamics description of nonNewtonian fluids," Acta Rheol. **43**, 502 (2004).
[11] R. C. Sharma, "Effect of rotation on thermal instability of a viscoelastic fluid," Acta Phys. Hungarica **40**, 11 (1976).
[12] R. C. Sharma and Sharma, "Thermal instability of an Oldroydian fluid with suspended particles in hydromagnetics in porous medium," Polym. Plast. Technol. Eng. **33**(3), 323 (1994).
[13] L. M. Pérez, J. Bragard, D. Laroze, J. Martinez-Mardones, and H. Pleiner, "Thermal convection thresholds in an Oldroyd magnetic fluid," J. Magn. Magn. Mater. **323**, 691 (2011).

Published under license by AIP Publishing.

[14]L. M. Pérez, J. Bragard, P. Díaz, H. L. Mancini, D. Laroze, and H. Pleiner, "Magneto-viscous effect on thermal convection thresholds in an Oldroyd magnetic fluid," J. Magn. Magn. Mater. **444**, 432 (2017).
[15]D. Laroze and H. Pleiner, "Thermal convection in a nonlinear non-Newtonian magnetic fluid," Commun. Nonlinear Sci. Numer. Simulat. **26**, 167 (2015).
[16]B. S. Bhadauria and P. Kiran, "Chaotic and oscillatory magneto-convection in a binary viscoelastic fluid under G-jitter," Int. J. Heat Mass Transf. **84**, 610 (2015).
[17]B. S. Bhadauria, "Chaotic convection in a viscoelastic fluid saturated porous medium with a heat source," J. Appl. Math. **2016**, 1487616.
[18]E. Ott, C. Grebogi, and J. A. Yorke, "Controlling chaos," Phys. Rev. Lett. **64**, 1196 (1990).
[19]K. Pyragas, "Continuous control of chaos by self-controlling feedback," Phys. Lett. A **170**, 421 (1992).
[20]K. Pyragas, "Delayed feedback control of chaos," Philos. Trans. R. Soc. A **364**, 2309 (2006).
[21]H. T. Yau and C. L. Chen, "Chaos control of Lorenz systems using adaptive controller with input saturation," Chaos Solitons Fractals **34**, 1567 (2007).
[22]W. M. Bessa, A. S. de Paula, and M. A. Savi, "Chaos control using an adaptive fuzzy sliding mode controller with application to a nonlinear pendulum," Chaos Solitons Fractals **42**, 784 (2009).
[23]M. N. Mahmud and I. Hashim, "Small and moderate Prandtl number chaotic convection in porous media in the presence of feedback control," Transp. Porous Media **84**, 421 (2010).
[24]M. N. Mahmud and I. Hashim, "Small and moderate Vadasz number chaotic convection in porous media in the presence of non-Boussinesq effects and feedback control," Phys. Lett. A **375**, 2382 (2011).
[25]R. Roslan, M. N. Mahmud, and I. Hashim, "Effects of feedback control on chaotic convection in fluid-saturated porous media," Int. J. Heat Mass Transf. **54**, 404 (2011).
[26]M. N. Mahmud, "Stability enhancement of high Prandtl number chaotic convection in an anisotropic porous layer with feedback control," J. Phys.: Conf. Ser. **1011**, 012081 (2018).
[27]Q. L. Sun, S. W. Wang, M. L. Zhao, C. Yin, and Q. Y. Zhang, "Weak nonlinear analysis of Darcy-Brinkman convection in Oldroyd-B fluid saturated porous media under temperature modulation," Int. J. Heat Mass Transf. **138**, 244 (2019).
[28]V. Ali, T. Gul, S. Afridi, F. Ali, S. O. Alharbi, and I. Khan, "Thin film flow of micropolar fluid in a permeable medium," Coating **138**, 244 (2019).
[29]M. A. Hassan, "Linear instability of viscoelastic nanofluid microjet with the effect of Marangoni convection," Phys. Scr. **94**, 025701 (2019).
[30]Z. Chaich, S. Saouli, and I. Rezayguia, "Thermodynamic analysis of viscoelastic fluid in a porous medium with presecribed wall heat flux over stretching sheet subjected to a transitive magnetic field," Therm. Sci. **23**, 219 (2019).
[31]G. R. Kefayati, G. R. Kefayati, H. Tang, A. Chan, and X. Wang, "A lattice Boltzmann model for thermal non-Newtonian fluid flows through porous media," Comput. Fluids **176**, 226 (2018).
[32]S. Kondo, H. Gotod, T. Miyano, and I. T. Tokuda, "Chaotic dynamics of large-scale double-diffusive convection in a porous medium," Phys. D Nonlinear Phenom. **364**, 1 (2018).
[33]M. M. Khader and S. Mziou, "Chebyshev spectral method for studying the viscoelastic slip flow due to a permeable stretching surface embedded in a porous medium with viscous dissipation and non-uniform heat generation," Boundary Value Prob. **2017**, 37 (2017).
[34]I. S. Shivakumara, M. Dhananjaya, and C.-O. Ng, "Thermal convective instability in an Oldroyd-B nanofluid saturated porous layer," Int. J. Heat Mass Transf. **84**, 167 (2015).
[35]J. A. C. Gallas, "Structure of the parameter space of the Hénon map," Phys. Rev. Lett. **70**, 2714 (1993).
[36]J. A. C. Gallas, "Stability diagrams for a memristor oscillator," Eur. Phys. J. Spec. Top. **228**, 2081 (2019), and references therein.
[37]T. Tang and H. H. Bau, "Stabilization of the no-motion state in the Rayleigh-Bénard problem," Proc. R. Soc. Lond. A **447**, 587 (1994).
[38]H. H. Bau, "Control of Marangoni-Bénard convection," Int. J. Heat Mass Transf. **42**, 1327 (1999).
[39]L. Storesletten, D. Andrew, and S. Rees, "The onset of convection in a viscoelastic liquid saturated anisotropic porous layer," Transp. Porous Media **67**, 203 (2007).
[40]L. J. Sheu, L.-M. Tam, J. H. Chen, H. K. Chen, and Y. K. Lin, "Chaotic convection of viscoelastic fluids in porous media," Chaos Solitons Fractals **37**, 113 (2008).
[41]J. Vadasz, J. E. A. Roy-Aikins, and P. Vadasz, "Sudden or smooth transitions in porous media natural convection," Int. J. Heat Mass Transf. **48**, 1096 (2005).
[42]P. Vadasz, J. H. Chen, H. K. Chen, and Y. K. Lin, "Instability and route to chaos in porous media convection," Fluids **2**, 26 (2017).
[43]E. N. Lorenz, "Deterministic nonperiodic flow," J. Atmos. Sci. **20**, 130 (1963).
[44]C. Sparrow, *The Lorenz Equations: Bifurcations, Chaos, and Strange Attractors*, 2nd ed. (Springer, Germany, 1982).
[45]P. G. Siddheshwar, G. N. Sekhar, and G. Jayalatha, "Effect of time-periodic vertical oscillations of the Rayleigh-Bérnard system on nonlinear convection in viscoelastic liquids," J. Nonnewton. Fluid Mech. **165**, 1412 (2010).
[46]M. Narayana, P. Sibanda, P. G. Siddheshwar, and G. Jayalatha, "Linear and nonlinear stability analysis of binary viscoelastic fluid convection," Appl. Math. Model. **37**(16–17), 8162–8178 (2013).
[47]A. Wolf, J. B. Swift, H. L. Swinney, and J. A. Vastano, "Determining Lyapunov exponents from a time series," Physica D, **16**, 285 (1985).
[48]J. C. Sprott, *Chaos and Time-Series Analysis* (Oxford University Press, Oxford, UK, 2003).
[49]O. E. Rössler, "An equation for hyperchaos," Phys. Lett. A **71**, 155 (1979).
[50]Q. Jia, "Hyperchaos generated from the Lorenz chaotic system and its control," Phys. Lett. A **366**, 217 (2007).
[51]D. Urzagasti, D. Becerra-Alonso, L. M. Pérez, H. L. Mancini, and D. Laroze, "Hyper-chaotic magnetisation dynamics of two interacting dipoles," J. Low Temp. Phys. **181**, 211 (2015).
[52]D. Laroze, J. Bragard, O. J. Suarez, and H. Pleiner, "Characterization of the chaotic magnetic particle dynamics," IEEE Trans. Mag. **47**, 3032 (2011).
[53]D. Laroze, D. Becerra-Alonso, J. A. C. Gallas, and H. Pleiner, "Magnetization dynamics under a quasiperiodic magnetic field," IEEE Trans. Mag. **48**, 3567 (2012).
[54]C. Kanchana, Y. Zhao, and P. G. Siddheshwar, "A comparative study of individual influences of suspended multiwalled carbon nanotubes and alumina nanoparticles on Rayleigh-Benard convection in water," Phys. Fluids **30**, 084101 (2018).
[55]G. C. Layek and N. C. Pati, "Bifurcations and hyperchaos in magnetoconvection of non-Newtonian fluids," Int. J. Bifurcat. Chaos **28**, 1830034 (2018).
[56]D. Laroze, P. G. Siddheshwar, and H. Pleiner, "Chaotic convection in a ferrofluid," Commun. Nonlinear Sci. Numer. Simul. **18**, 2436 (2013).
[57]G. C. Layek and N. C. Pati, "Bifurcations and chaos in convection taking non-Fourier heat-flux," Phys. Lett. A **381**, 3568 (2017).
[58]J. G. Freire and J. A. C. Gallas, "Stern-Brocot trees in the periodicity of mixed-mode oscillations," Phys. Chem. Chem. Phys. **13**, 12191 (2011).
[59]J. Park, H. Lee, Y. Jeon, and J. Baik, "Periodicity of the Lorenz-Stenflo equations," Phys. Scr. **90**, 065201 (2015).
[60]P. C. Rech, "Organization of the periodicity in the parameter-space of a glycolysis discrete-time mathematical model," J. Math. Chem. **57**, 632–637 (2019).
[61]D. Roy and Z. E. Musielak, "Generalized Lorenz models and their routes to chaos. III. Energy-conserving horizontal and vertical mode truncations," Chaos Solitons Fractals **33**, 1064–1070 (2007); "Generalized Lorenz models and their routes to chaos. II. Energy-conserving horizontal mode truncations," *ibid.* **31**, 747–756 (2007); "Generalized Lorenz models and their routes to chaos. I. Energy-conserving vertical mode truncations," *ibid.* **32**, 1038–1052 (2007).

Published under license by AIP Publishing.